

# Automated tissue segmentation of MR brain images in the presence of white matter lesions

Sergi Valverde<sup>a,\*</sup>, Arnau Oliver<sup>a</sup>, Eloy Roura<sup>a</sup>, Sandra González<sup>a</sup>, Deborah Pareto<sup>b</sup>, Joan C. Vilanova<sup>c</sup>, Lluís Ramió-Torrentà<sup>d</sup>, Àlex Rovira<sup>b</sup>, Xavier Lladó<sup>a</sup>

<sup>a</sup>Research institute of Computer Vision and Robotics, University of Girona, Spain

<sup>b</sup>Magnetic Resonance Unit, Dept of Radiology, Vall d'Hebron University Hospital, Spain

<sup>c</sup>Girona Magnetic Resonance Center, Spain

<sup>d</sup>Multiple Sclerosis and Neuroimmunology Unit, Dr. Josep Trueta University Hospital, Spain

---

## Abstract

During the last years, the increasingly interest of brain tissue volume measurements on clinical settings has lead to the development of a wide number of automated tissue segmentation methods. However, white matter lesions are known to reduce the accuracy of automated tissue segmentation methods, which requires to manually annotate lesions and refill them before segmentation, which is tedious and time-consuming. Here, we propose a new fully automated T1-w/FLAIR tissue segmentation approach designed to deal with images in the presence of WM lesions, which integrates a robust partial volume tissue segmentation with WM outlier rejection and filling, combining intensity, probabilistic and morphological prior maps. We evaluate the accuracy of the method on the MRBrainS13 tissue segmentation challenge database, and also on a set of Multiple Sclerosis (MS) patient images. On both databases, we validate the performance of our method with other state-of-the-art techniques. On the MRBrainS13 data, the presented approach was the best unsupervised ranked method of the challenge (7th position) and clearly outperformed other unsupervised pipelines such as *FAST* and *SPM12*. On MS data, the differences in tissue segmentation between the images segmented with our method and the same images where manual expert annotations were used to refill lesions on T1-w images before segmentation were lower or similar to the best state-of-the-art pipeline incorporating automated lesion segmentation and filling. Our results show that the proposed pipeline quantitatively improved the accuracy of tissue segmentation while it achieved very competitive results on MS images. A public version of the approach is available to download for the neuro-imaging community.

**Keywords:** Brain, MRI, multiple sclerosis, automatic tissue segmentation, white matter lesions

---

## 1. Introduction

Brain tissue volume based on Magnetic Resonance Imaging (MRI) is increasingly being used in clinical settings to assess brain volume in different neurological dis-

eases such as the Multiple Sclerosis (MS) (Giorgio and De Stefano, 2013). In MS, several studies have analyzed the histopathological changes of patients with respect to the progression of the disease, showing that the percentage of change in brain volume tends to correlate with worsening conditions (Pérez-Miralles et al., 2013; Sormani et al., 2014). However, manual segmentation of brain tissue is both challenging and time-consuming because of the large number of MRI slices for each patient which composes the three-dimensional information, and the inher-

---

\*Corresponding author. S. Valverde, Ed. P-IV, Campus Montilivi, University of Girona, 17071 Girona (Spain). e-mail: svalverde@eia.udg.edu. Phone: +34 972 418878; Fax: +34 972 418976.

ent intra/inter-observer variability of manually segmented scans (Cabezas et al., 2011). The development of automated MS tissue segmentation methods that can segment large amounts of MRI data, do not suffer from intra/inter-observer variability and specific changes of the brain such as MS associated lesions and brain atrophy are still an active research field (Klauschen et al., 2009; de Bresser et al., 2011; Valverde et al., 2015a; Vincken et al., 2015).

Different brain tissue segmentation methods have been used in MS so far. General purpose intensity based methods combining intensity and a priori statistical anatomic information such as FAST (Zhang et al., 2001) or SPM (Ashburner and Friston, 2005) are nowadays widely used. However, tissue abnormalities found in MS image patients such as White Matter (WM) lesions reduce the accuracy of these techniques (Chard et al., 2010; Battaglini et al., 2012) usually causing an overestimation of Gray Matter (GM) tissue not only by the effect of hypo-intense WM lesion voxels classified as GM, but also by the effect of these lesion voxels in normal-appearing tissue (Valverde et al., 2015b). In these cases, in-painting lesions on the T1-weighted image (T1-w) with signal intensities of the normal-appearing WM before tissue segmentation may be used to reduce the effects of WM lesions on tissue segmentation (Chard et al., 2010; Battaglini et al., 2012; Valverde et al., 2014). However, MS lesions have to be delineated manually first, which may be tedious, challenging and time-consuming task depending of the characteristics of the image (Lladó et al., 2012).

Regarding this issue, a wide number of automated lesion segmentation techniques have been proposed during the last years (Lladó et al., 2012; García-Lorenzo et al., 2013). Most of these methods integrate other imaging modalities such as T2-weighted, Proton Density (PD) and Fluid Attenuated Inverse Recovery (FLAIR), as these modalities present a high contrast between tissue and lesions (Lladó et al., 2012). More recent techniques include supervised learning classifiers based on spatial decision forest (Geremia et al., 2011), statistical methods (Sweeney et al., 2013), patch-based models (Guizard et al., 2015) or adaptive dictionary learning methods (Deshpande et al., 2015). Further, different unsupervised learning techniques make use of probabilistic models to separate WM lesions from normal-appearing tissue by considering lesions as an outlier class (Harmouche et al., 2015; Tomas-Fernandez and Warfield, 2015; Jain et al.,

2015). Also, other unsupervised techniques make use of the signal intensity of lesions on FLAIR several thresholding methods with post-processing steps to automatically segment lesions (Schmidt et al., 2012; Roura et al., 2015). In contrast, there are fewer studies that have been focused on the tissue segmentation of MS images containing lesions. Those include non-supervised techniques combining intensity, anatomical and morphological maps (Nakamura and Fisher, 2009; Shiee et al., 2010), or supervised methods such as statistical classifiers (Datta and Narayana, 2013), atlas based nearest-neighbor methods (De Boer et al., 2009) and sparse dictionary learning approaches (Roy et al., 2015).

The increasing amount of published studies regarding automated WM lesion segmentation may be given by the particular need of a quantitative analysis of focal MS lesions in individual and temporal studies (Lladó et al., 2012). Recent studies in MS (Chard et al., 2010; Gelineau-Morel et al., 2012; Ceccarelli et al., 2012; Pérez-Miralles et al., 2013; Popescu et al., 2014; Magon et al., 2014; Valverde et al., 2015b) indicate a certain tendency to the use of widely validated segmentation tools such as Siena (Smith et al., 2002), FAST (Zhang et al., 2001) or SPM (Ashburner and Friston, 2005) in combination with automated lesion segmentation and/or lesion-filling approaches, although their application in clinical practice is still not generalized (Giorgio and De Stefano, 2013).

In this paper, we present the Multiple Sclerosis SEGmentation pipeline (*MSSEG*), a novel multi-channel method designed to segment GM, WM and cerebro-spinal fluid (CSF) tissues in images of MS patients. This method is motivated by our previous analysis of the effects of tissue segmentation on MS images (Valverde et al., 2015b), the role of lesion-filling (Valverde et al., 2014), and its combination with automated lesion segmentation on tissue segmentation (Valverde et al., 2015b). Similar to the works of Nakamura and Fisher (2009) and Shiee et al. (2010), our approach utilizes a combination of intensity, anatomical and morphological prior maps to guide the tissue segmentation. However, tissue segmentation is here based on a robust partial volume segmentation where WM outliers are estimated and refilled before segmentation using a multi-channel post-processing algorithm. This post-processing algorithm is partially inspired on MS lesion segmentation algorithm

proposed by Roura et al. (2015), but here we integrate multi-channel support, partial volume segmentation, spatial context, and prior anatomical and morphological atlases. In order to perform quantitative and qualitative evaluations of our approach, we analyze its accuracy with the MRBrainS13 challenge database which includes manual tissue annotations, and also with a set of MS patient images with different lesion burden. We quantitatively compare the performance of our approach with different state-of-the-art techniques that also competed on the MRBrainS13 challenge and/or have been used in recent MS studies. Furthermore, we also analyze the differences in the performance of our approach when using only T1-w or when using the multi-channel approach that includes T1-w and FLAIR. The *MSSEG* method is currently available for download at our research group webpage (<http://atc.udg.edu/nic/msseg/index.html>).

## 2. Methods

The proposed brain tissue segmentation method is composed of five different processes: registration of statistical atlas into T1-w space (Sec. 2.2), tissue estimation (Sec. 2.3), detection and re-assignation of lesion candidate to T1-w (Sec. 2.4), tissue re-estimation, and partial volume re-assignation of tissue maps into CSF, GM and WM (Sec. 2.5). The overall schema of the pipeline is depicted in figure 1. We describe each step in detail in the following subsections.

### 2.1. Notation

To describe our proposed approach, we employ the following notation.  $T$  and  $F$  denote the input images T1-w and FLAIR, respectively.  $P^c$  denotes a probabilistic tissue atlas of particular class  $c = \{csf, csfgm, gm, gmwm, wm\}$ .  $S^{st}$  denotes a morphological brain atlas of a particular parcellated structure  $st$ . For each of the above images,  $T_j, F_j, P_j^c$  and  $S_j^{st}$  denote an observation at a voxel  $j \in \Omega$ , being  $\Omega$  the image domain.

### 2.2. Tissue prior registration

The MNI-ICBM 152 2009a Nonlinear T1-w average structural template image<sup>1</sup> was first affine registered to

the native T1-w image space based on a block matching approach (Ourselin et al., 2002), and then non-rigid registered with a fast free-form deformation method (Modat et al., 2010), both using the Nifty Reg package<sup>2</sup>. Obtained transformation parameters were then used to resample the available MNI CSF, GM and WM tissue priors to the T1-w space. The resampled probabilistic tissue maps  $P^{csf}$ ,  $P^{gm}$  and  $P^{wm}$  were extended to build intermediate partial volumes  $P_{csfgm}^{csm}$  as  $(P^{csf} \geq 0.5 \cap P^{gm} \geq 0.5)$  and  $P_{gmwm}^{csm}$  as  $(P^{gm} \geq 0.5 \cap P^{wm} \geq 0.5)$  and taking the mean value of the two input atlases.

Besides, a morphological brain structure atlas was first parcellated on the original MNI atlas using the hierarchical algorithm proposed by Pohl et al. (2007) on EM-Segmenter<sup>3</sup>, and then manually refined for the selected structures. The resulting atlas ( $S^{st}$ ) consisted of useful structures for tissue segmentation such as cortical GM ( $S^{Cortex}$ ), ventricles ( $S^{VENT}$ ), basal ganglia ( $S^{BASAL}$ ) and brainstem ( $S^{BRAINSTEM}$ ). The same transformation parameters were also used to resample the morphological atlas to the T1-w space.

### 2.3. Tissue estimation

Brain tissue was estimated following a robust fuzzy-clustering approach similar to the one proposed in Pham (2001), as this method provides a straightforward implementation, fairly robust behavior including spatial context information, applicability to multichannel data, and the ability to model uncertainty within the data (Pham, 2001). In our approach, we designed the method to segment 5 classes in order to preserve better the differences in signal intensity between local regions of the brain and lesion candidates. We also extended the spatial penalizing weights by incorporating the probabilistic tissue priors in the segmentation process similarly to Shiee et al. (2010). Hence we modified the objective function proposed by Pham (2001) in order to incorporate also prior-atlas information as follows:

<sup>2</sup><http://cmictig.cs.ucl.ac.uk/wiki/index.php/NiftyReg>

<sup>3</sup><https://www.slicer.org/slicerWiki/index.php/EMSegmenter-Overview>

<sup>1</sup><http://www.bic.mni.mcgill.ca/ServicesAtlases/ICBM152NLin2009>

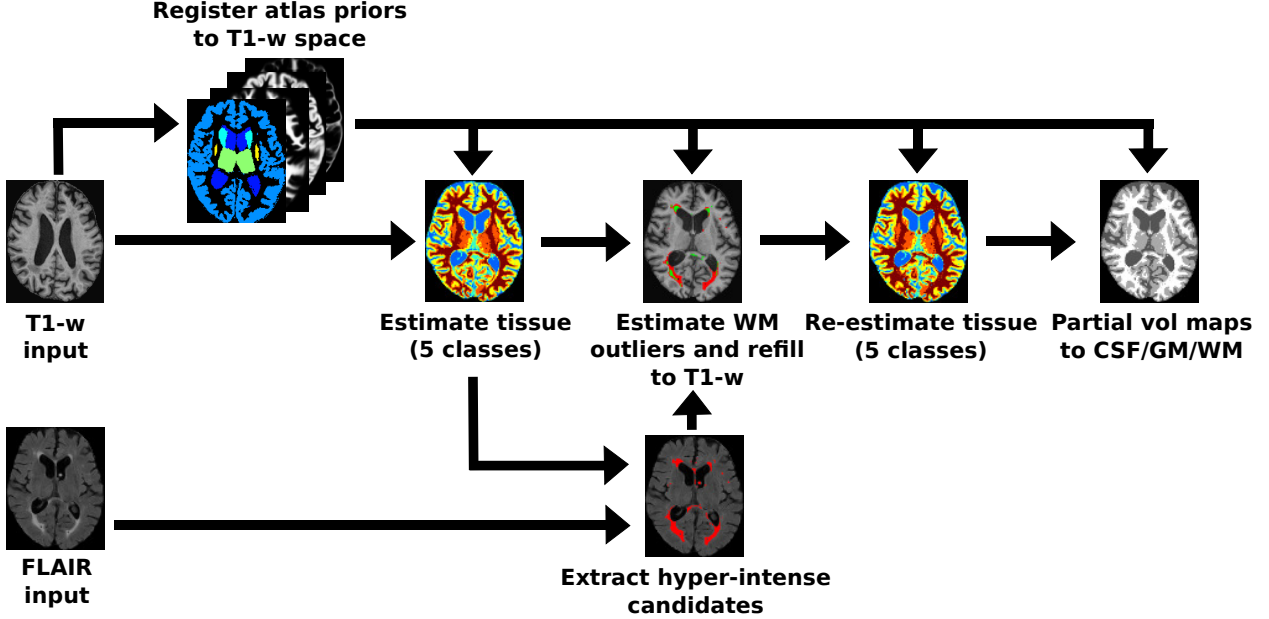


Figure 1: The proposed method *MSSEG* consists of five different steps: 1) Three statistical *a-priori* tissue atlases (CSF, GM and WM) and a brain structure atlas are first registered into the patient space (Sec. 2.2) and then used to 2) guide the tissue segmentation of the input T1-w image (Sec. 2.3). 3) Then, the same output segmentation is employed to detect and reassign candidate regions into WM based on the registered *a-priori* and hyper-intense FLAIR maps if available (Sec. 2.4). The voxel intensities of candidate regions on T1-w are then refilled with normal-appearance WM intensities and 4) tissue is re-estimated (Sec. 2.3). 5) Finally, intermediate volume maps are reassigned into CSF, GM and WM using both neighbor and spatial prior information (Sec. 2.5).

$$\begin{aligned}
J_{MSSEG} = & \sum_{j \in \Omega} \sum_{k=1}^C u_{jk}^q \|T_j - v_k\|^2 + \\
& + \frac{\beta}{2} \sum_{j \in \Omega} \sum_{k=1}^C u_{jk}^q \sum_{l \in N_j^w} \sum_{m \in M_k} u_{lm}^q + \\
& + \frac{\gamma}{2} \sum_{j \in \Omega} \sum_{k=1}^C u_{jk}^q \sum_{l \in N_j^w} \sum_{m \in M_k} P_l^k
\end{aligned} \quad (1)$$

where  $\{k \in C \mid C = \{csf, csfgm, gm, gmwm, wm\}\}$ ,  $u_{jk}$  denotes the membership probability of each voxel  $j$  for a particular class,  $v_k$  are the cluster signal intensity centers of each class,  $N_j^w$  is the set of two-dimensional (2D)  $(2w+1)^2$  or three-dimensional (3D)  $(2w+1)^3$  neighbors centered on the voxel  $j$ , and  $M_k = \{1, \dots, C\} \setminus \{k\}$ . This approach depends on four parameters to adjust the membership functions: the weighting parameter  $q$  that controls the degree of fuzziness, the spatial constraint parameter  $\beta$  that controls the amount of neighbor information added, the prior belief parameter  $\gamma$  used to control the amount of prior atlas information about each tissue, and finally the window radius of neighbors  $w$ .

Similar to the work of Pham (2001), an iterative algorithm to minimize (1) was derived by evaluating the cen-

troids and the functions that satisfy a zero gradient condition as follows:

---

#### Algorithm 1 Tissue estimation

---

- 1: Obtain the initial estimates of the centroids for each class  $k = \{1, \dots, C\}$ :  

$$v_k = \frac{1}{n} \sum_{j \in \Omega} (T_j^k \mid P_j^k \geq 0.5) \quad n = |(T_j^k \mid P_j^k \geq 0.5)|$$
  - 2: Compute the membership functions  $u_{jk}$
  - 3: Compute the new centroids:  

$$v_k = \frac{\sum_{j \in \Omega} u_{jk}^q T_j}{\sum_{j \in \Omega} u_{jk}^q} \quad k = \{1, \dots, C\}$$
  - 4: Repeat steps 2 and 3 until convergence
- 

Initial centroids  $v_k$  were estimated for each class  $C$  by taking the mean signal intensity of the voxels on the T1-w image with prior-tissue probability  $P_j^k \geq 0.5$ . The membership function  $u_{jk}$  was also adapted to incorporate prior-atlas information and computed as follows:

$$u_{jk} = \frac{(\|T_j - v_k\|^2 + \beta \sum_{l \in N_j} \sum_{m \in M_k} u_{lm}^q + \gamma \sum_{l \in N_j} \sum_{m \in M_k} P_l^m)^{-1/(q-1)}}{\sum_{i=1}^C (\|T_j - v_i\|^2 + \beta \sum_{l \in N_j} \sum_{m \in M_i} u_{lm}^q + \gamma \sum_{l \in N_j} \sum_{m \in M_i} P_l^m)^{-1/(q-1)}} \quad (2)$$

The five classes tissue segmentation mask  $SEG_j$  was

computed by assigning to each voxel the class with maximum membership as follows:

$$SEG_j = \arg \max_k u_{jk} \quad \forall j \in \Omega \quad (3)$$

The parameters  $q$ ,  $\gamma$  and  $w$  can be tuned manually to increase the performance of the method, but were set to default values  $q = 2$ ,  $\gamma = 0.1$  and  $w = 1$  with 2D that worked well in the majority of cases. In contrast, the  $\beta$  parameter depends on the brightness of the image, the deviation of the signal intensities of voxel class members with respect to their centroid value, and image noise (Pham, 2001). Hence, choosing a proper value for the  $\beta$  parameter was important to obtain optimal or near-optimal performance. In our implementation, we automated the choose of the  $\beta$  parameter by fitting a function of the optimal empirical selection of the parameter with respect to different levels of noise. To do so, we estimated iteratively the sub-optimal  $\beta$  parameter of 10 images of the Brainweb dataset<sup>4</sup> that included different noise level (1-9%) and ground-truth annotations. For each image, we also computed the noise level using the Fast Noise Variance method proposed by Immerkær (1996). Then, the correspondent  $\beta$  parameters and noise levels were used to fit a polynomial function to interpolate the  $\beta$  parameter. For all the evaluated images in the paper, we have automatically approximated the  $\beta$  as a function  $B(x)$  of their noise level  $x$  as  $B(x) = 0.0011x^4 - 0.0015x^3 + 0.0074x^2 - 0.001x + 0.05$ .

#### 2.4. Reassign WM outliers to T1-w

In a three class tissue segmentation approach, lesion regions are usually classified as either GM or WM, given the hypo-intense signal intensity profile of WM lesions. This impedes in some cases to differentiate them from surrounding GM and WM. In contrast, by creating the intermediate classes *CSFGM* and *GMWM*, new local clusters of voxels with similar signal intensities are delimited, increasing the chances that WM lesion regions may be differentiated from normal-appearing GM and WM. Following this assumption, we estimated WM lesion regions by analyzing all local regions not initially segmented as WM based on their the prior probability and the spatial connection to WM.

---

<sup>4</sup><http://brainweb.bic.mni.mcgill.ca/brainweb/>

First, different binary segmentation masks  $M^c$  were computed for each of the classes  $c = \{gmwm, gm, csfgm\}$ . For each mask, all 2D regions of connected components were computed using a flood-fill algorithm with 4-connected neighborhood. We define the set of all 4-connected  $p$  regions given an input binary image as follows:

$$R_p^T \leftarrow \oplus(M_j^c, n), \quad p = \{1, \dots, |R_p^T|\}$$

where the operator  $\oplus$  refers to the connected components function and  $n$  is the number of connected neighbors.

Secondly, a map of hyper-intense region candidates was computed on the FLAIR image following the same strategy shown in Roura et al. (2015). The binary mask  $M^{GM}$  was first used to compute the intensity distribution on the FLAIR image, where GM is typically hyper-intense with respect to CSF and WM, and WM lesions are considered hyper-intense outliers to GM. The mean and standard deviation of the GM distribution was computed using the full-width at half maximum (FWHM) of the main peak of a generated histogram. Then, an initial map of hyper-intense regions voxels  $H^{FLAIR}$  was determined by thresholding the FLAIR image  $F$  as follows:

$$H_j^{FLAIR} = \begin{cases} 1 & \text{if } F_j > \mu + \alpha\sigma \\ 0 & \text{otherwise} \end{cases} \quad \forall j \in \Omega \quad (4)$$

where  $\mu$  and  $\sigma$  were the mean and standard deviation, respectively, of the GM distribution as computed using the FWHM, and  $\alpha$  was a weighting parameter that scaled the minimum signal intensity of outliers. The binary mask  $H^{FLAIR}$  was then used to group the candidate voxels into connected regions using the same method proposed before:

$$R_t^F \leftarrow \oplus(H^{FLAIR}, n), \quad t = \{1, \dots, |R_t^F|\}$$

where  $n$  was set to 3D connected elements ( $n = 6$ ) in order to reduce the amount of 2D false positive regions such as hyper-intense sub-arachnoid tissue.

Given the computed binary masks for each tissue  $M^{gmwm}$ ,  $M^{gm}$  and  $M^{csfgm}$ , the map of hyper-intense voxels on FLAIR  $H^{FLAIR}$ , and its connected components  $R_t^F$ , we used an iterative algorithm to estimate the regions with

high probability to pertain to WM. Lesion filling of selected regions was integrated in the same algorithm. Figure 2 shows in detail each of the steps of the algorithm. Regions not overlapping cortical GM on the morphological prior  $S_s^{CORTEX}$  were only processed if a matched region was also hyper-intense in FLAIR, in order to reduce the amount of false positive regions such as isolated cortical GM segmented regions. Regions not touching cortical GM were filtered based on their prior probability to pertain to WM and their distance to surrounding WM. If half of the voxels of a region had a prior probability to pertain to WM and the region was connected to actual WM, the region was also added to the WM class, and those voxels were refilled as normal-appearing WM into the original T1-w image  $T$  using the same implementation proposed in Valverde et al. (2014). Note that classes were visited from *gmwm* to *csfgm* in order to add new belief of the actual WM and use it to filter next regions.

If the FLAIR modality is not available,  $H^{FLAIR}$  is automatically set to zero, disabling the evaluation of  $R^H$  regions and henceforth forcing the method to evaluate the next T1 region  $R_p^T$ . If FLAIR is used, all regions that were discarded on the first part of the algorithm or overlapped the cortex, were filtered according to their spatial attributes on the FLAIR image. Each discarded region  $R_q^T$  on the segmented mask  $SEG$  was matched with a particular region in FLAIR  $R_t^F$  based on their overlap ( $R_t^F \mid t = \arg \max(|R_t^F \cap R_q^T|)$ ). Then, matched regions where half of their surrounding neighbors were actually classified as *gmwm* or *wm* were also added to the WM class and T1-w filled. In all cases, we referred to the neighboring voxels of a region  $N_S$  as the neighbors with one voxel of distance from the region boundaries.

## 2.5. Partial volume maps

Once WM outliers were reassigned to T1-w, the resulting refilled image was used to estimate the brain tissue following the same method described in Sec. 2.3. Afterwards, partial volume maps (*csfgm*) and (*gmwm*) were reassigned to each of the three main classes CSF, GM and WM following a region-wise approach.

Local 2D regions with similar intensity that were classified as *csfgm* and *gmwm* were estimated using the same connected component algorithm described before. The structural brain atlas  $S$  was then used to reassign regions

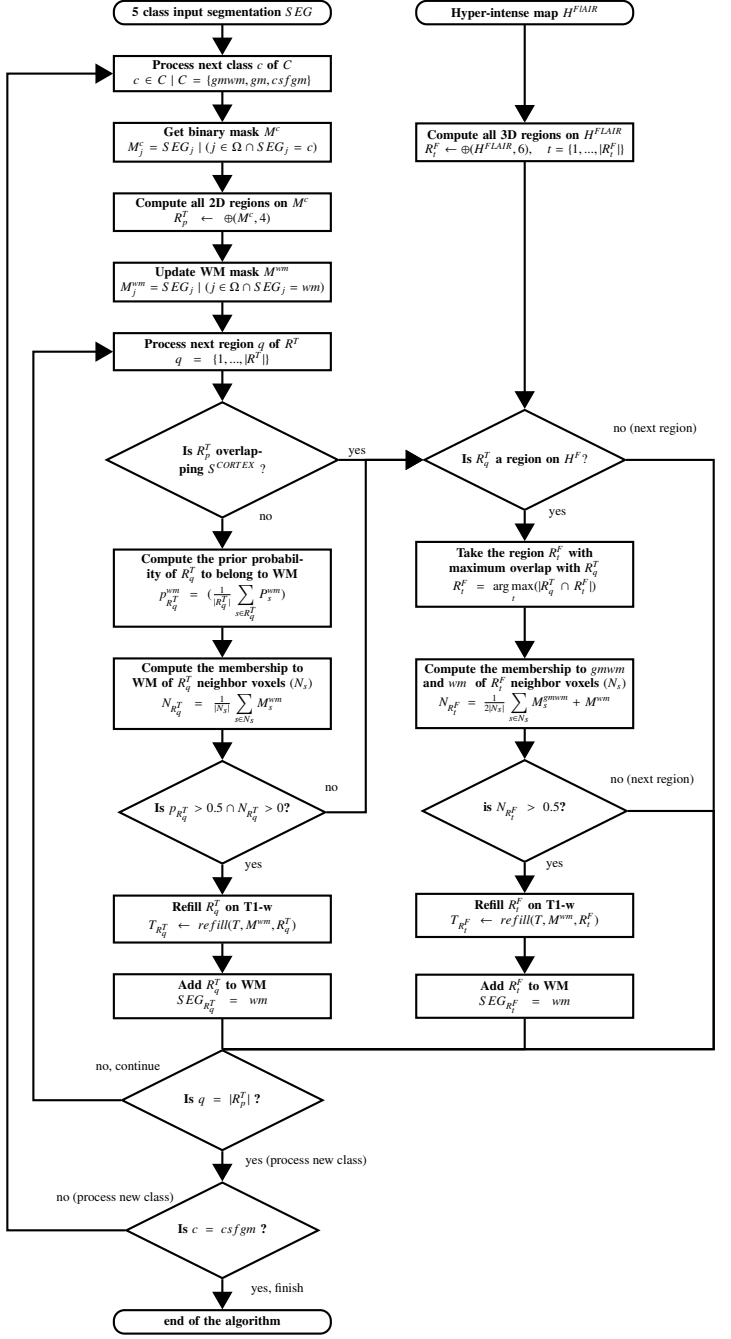


Figure 2: Proposed algorithm to estimate and refill outlier candidate regions into T1-w. The algorithm takes the 5 a class T1-w segmentation and the hyper-intensity map  $H^{FLAIR}$  if available as inputs. Connected regions of voxels with similar intensity are filtered based on their spatial location probability on tissue and morphological prior atlases. Selected regions are then refilled on the original T1-w image.

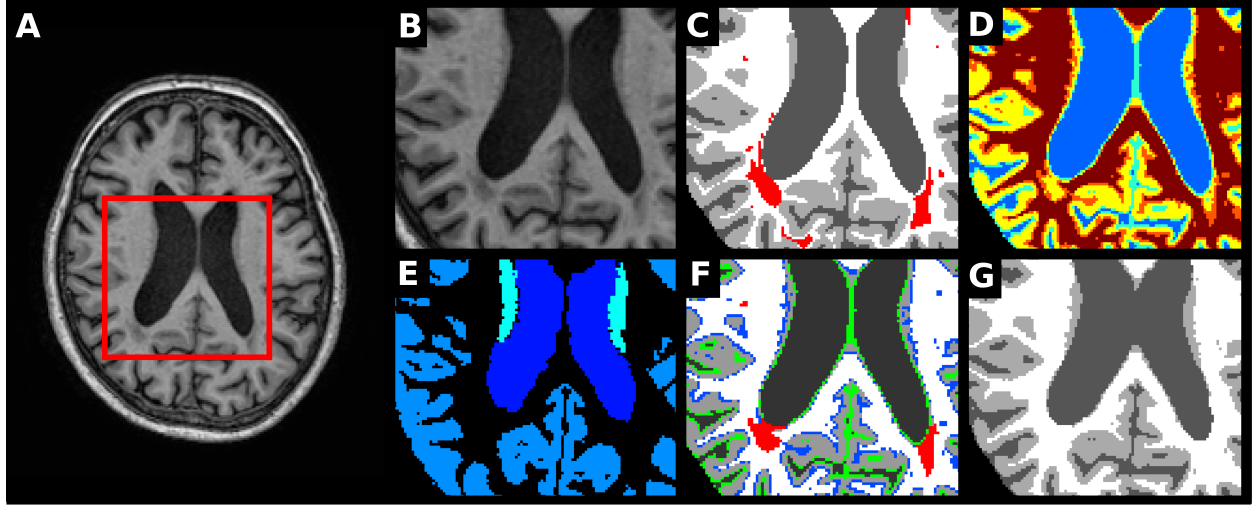


Figure 3: Partial volume assignment during tissue segmentation (Sec. 2.5). A) Original T1-w image. B) Detailed view of the T1-w image. C) Tissue ground-truth with WM lesions highlighted in red. D) Initial 5 class tissue segmentation where *csf*, *csfgm*, *gm*, *gmwm* and *wm* tissues are depicted in blue, cyan, yellow, orange and red, respectively (see Sec. 2.3). E) Morphological brain tissue atlas with parcellated GM regions and ventricles. F) Partial volume *csfgm* and *gmwm* regions (depicted in green and blue, respectively). Previously estimated lesion candidates are depicted in red (see Sec. 2.4). 2D regions with half of their voxels overlapping with the morphological atlas are reassigned to the correspondent tissue. The rest of voxels are reassigned to the neighboring pure class with the most similar signal intensity. G) Final tissue segmentation with partial tissue volume maps re-estimated as CSF (dark gray), GM (light gray) and WM (white).

that at least half of their voxels overlapped with certain structures as follows:

$$SEG_{R_p} = \begin{cases} CSF & \text{if } \left( \frac{1}{|R_p|} \sum_{s \in R_p} S_s^{VENT} \right) > 0.5 \\ GM & \text{if } \left( \frac{1}{2|R_p|} \sum_{s \in R_p} S_s^{Cortex} + S_s^{BASAL} \right) > 0.5 \\ WM & \text{if } \left( \frac{1}{|R_p|} \sum_{s \in R_p} S_s^{BRAINSTEM} \right) > 0.5 \end{cases} \quad (5)$$

for all the regions  $p = \{1, \dots, |R_p|\}$ . The rest of voxels not reassigned previously were reclassified by adding them to the surrounding pure class with the most similar intensity as follows:

$$SEG_j = \arg \min_c \left| T_j - \frac{1}{|N_j|} \sum_{s=1}^{|N_j|} (T_s \mid SEG_s = c) \right| \quad (6)$$

for pure classes  $c = \{csf, gm, wm\}$  and partial volume voxels  $j = \{\forall j \in \Omega \mid SEG_j = csfgm \cup gmwm\}$ . The radius for neighbor voxels was set to 6 in two dimensions. Figure 3 depicts the partial volume re-assigment process for one particular T1-w image.

### 3. Experiments

#### 3.1. MRBrainS database

##### 3.1.1. Data

The public available MRBrainS 2013 database<sup>5</sup> consisted of 20 scans with varying degree of brain atrophy and white matter lesions. These scans were acquired on a 3.0T Philips Achieva MR scanner at the University Medical Center Utrecht (The Netherlands) with the following sequences: 3D T1-w (TR: 7.9ms, TE: 4.5ms), T1-Inverse Recovery (TR: 4416ms, TE: 15ms, and TI: 400ms), and T2-weighted/FLAIR (TR: 11000ms, TE: 125ms, and TI: 2800 ms). Each of the scans was co-registered (Klein et al., 2010) and intensity-corrected (Ashburner and Friston, 2005) before releasing the data. T1, T1-IR, and T2/FLAIR voxel size was  $(0.96 \times 0.96 \times 3.00 \text{ mm}^3)$  after registration (Vincken et al., 2015).

Three experts manually delineated each of the 20 scans into CSF, GM and WM and these annotations were used as the reference standard for the evaluation framework (Vincken et al., 2015). Extended manual annotation containing various brain structures and white matter lesions for 5 scans were provided for training while the remaining 15 scans were blind and had to be skull-stripped and segmented into CSF, GM and WM by participating teams.

<sup>5</sup>available for download at: <http://mrbrains13.isi.uu.nl/>

### 3.1.2. Evaluation:

Segmentation results had to be submitted online for external evaluation based on the following scores for the CSF, GM and WM tissues ( $c$ ):

- Dice similarity coefficient ( $DSC_c$ ) (Dice, 1945) between the manual tissue segmentation ( $GT_c$ ) and the computed segmentation ( $SEG_c$ ) masks:

$$DSC_c = \frac{2 |SEG_c \cap GT_c|}{|SEG_c| + |GT_c|} \times 100 \quad (7)$$

- The modified Hausdorff distance (95th percentile) (Huttenlocher et al., 1993) between the manual tissue segmentation ( $GT_c$ ) points  $p'$  and the computed segmentation points  $p$  in ( $SEG_c$ ) masks:

$$h_c^{95} = \max_{p \in SEG_c} \min_{p' \in GT_c} |p - p'| \quad (8)$$

- The absolute difference in tissue volume ( $AVD_c$ ) between manual tissue segmentation ( $GT_c$ ) and the computed segmentation ( $SEG_c$ ) masks:

$$AVD_c = \left\| \frac{|SEG_c| - |GT_c|}{|GT_c|} \right\| \quad (9)$$

In order to evaluate the performance of our method, we submitted two different segmentation sets using either only the T1-w sequences or both T1-w and FLAIR images. We validated the performance of our approach comparing the obtained scores with other submitted segmentation pipelines.

### 3.1.3. Parameter settings

Skull stripping of input images was performed using a similar approach to other methods participating in the challenge (Jog et al., 2013; Opbroek et al., 2013; Rajchl et al., 2015). The 5 training images were non-rigidly registered to the image space of each of the T1-w (Modat et al., 2010), and the brainmask was generated by simple voting of the registered masks. Afterwards, each mask was refined on the T1-IR image by thresholding hyperintense voxels.

All the parameters of our tissue segmentation method were set to default values ( $q = 2, \gamma = 0.1, w = 1$ ). The  $\beta$  parameter was computed automatically as described in Section 2.3. The  $\alpha$  parameter that scaled the minimum signal intensity on the  $H^F$  mask was set to  $\alpha = 3$ .

### 3.2. MS database

#### 3.2.1. Data

This non-public database of images was composed by 24 images of clinically isolated syndrome (CIS) patients acquired on a 3T Siemens MR scanner (Trio Tim, Siemens, Germany) with a 12-channel phased-array head coil (data from Hospital Vall D’Hebron, Barcelona, Spain). The following pulse sequences were obtained: 1) transverse proton density and T2-weighted fast spin-echo (TR=2500 ms, TE=16-91 ms, voxel size=0.78×0.78×3mm<sup>3</sup>); 2) transverse fast T2-FLAIR (TR=9000ms, TE=93ms, TI=2500ms, flip angle=120°, voxel size=0.49×0.49×3mm<sup>3</sup>); and 3) sagittal 3D T1 magnetization prepared rapid gradient-echo (MPRAGE) (TR=2300 ms, TE=2 ms; flip angle=9°; voxel size=1×1×1.2mm<sup>3</sup>). For each scan, T1-w and FLAIR images were first skull-stripped using BET (Smith, 2002) and then intensity-corrected using the N3 method (Sled et al., 1998). Finally, FLAIR images were co-registered into the T1-w space and then re-aligned into the MNI space using SPM12 co-registration tools with the normalized mutual information as objective function and tri-linear interpolation with no wrapping (Ashburner and Friston, 2005). White matter lesion masks were semi-automatically delineated from FLAIR using JIM software<sup>6</sup> by an expert radiologist of the hospital center. Mean lesion volume was  $4.30 \pm 4.84$  ml (range 0.1-18.3 ml).

#### 3.2.2. Evaluation

Manual expert annotations of tissues were not available for this database. As validated in previous MS studies (Battaglini et al., 2012; Valverde et al., 2015b,c), WM lesions on original T1-w scans were first refilled with signal intensities similar to normal-appearing WM using the SLF lesion filling method (Valverde et al., 2014). Then, both the original and the refilled images were segmented into CSF, GM and WM tissues using our proposed approach. The performance of our tissue segmentation method was evaluated by computing the absolute difference in tissue volume ( $AVD_c$ ) between the images segmented containing lesions and the same images where WM lesions were refilled before tissue segmentation:

---

<sup>6</sup>Xinapse Systems, <http://www.xinapse.com/home.php>

$$AVD_c = \left\| \frac{|SEG_c| - |GT_c^{fill}|}{|GT_c^{fill}|} \right\| \times 100 \quad (10)$$

where  $SEG_c$  refers to the output segmentation masks of the images segmented containing lesions, and  $GT_c^{fill}$  refers to the output tissue segmentation masks of images where lesions were filled before segmentation and considered as ground-truth.

Several works (DellOglio et al., 2014; Valverde et al., 2015c) have already shown that part of the actual error in tissue segmentation may be partially masked by opposite directions in the differences in total and normal-appearing tissue. In order to add an additional measure estimator of the actual error in tissue segmentation that may not bias by these differences, we also compared for each tissue the percentage of mis-classified voxels  $PMC_c$  between the original  $SEG_c$  and the expert filled  $GT_c^{fill}$  masks:

$$PMC_c = \frac{|\overline{SEG_c} \cap GT_c^{fill}|}{|GT_c^{fill}|} \times 100 \quad (11)$$

In order to analyze the benefits of using the FLAIR image into the proposed approach, we evaluated the performance of our method when using only the T1-w image and when using both T1-w and FLAIR. Furthermore, we validated it with two other automated pipelines widely used in brain tissue segmentation, such as FAST (Zhang et al., 2001) (version FSL 5.0) and SPM (Ashburner and Friston, 2005) (version SPM12 rev 6225), using either original images or after estimating lesions using the automated approach SLS proposed by Roura et al. (2015). On images where lesions were automatically segmented, estimated lesion masks were then filled with the same SLF method (Valverde et al., 2014) before tissue segmentation. Similarly to our approach, we considered the tissue segmentation masks of the expert refilled T1-w images segmented with FAST and SPM12 as the ground-truth for each method. Table 1 summarizes each of the evaluated pipelines and the corresponding process followed to segment the MS images.

### 3.2.3. Parameter settings

The BET skull-stripped process was optimized as proposed by Popescu et al. (2012) without removing CSF

Table 1: Summary of evaluated pipelines and processes used on MS data. On pipelines *FAST only T1* and *SPM12 only T1* images were segmented containing lesions without prior automated lesion segmentation. On pipelines *FAST + SLS* and *SPM12 + SLS*, WM lesions were automatically segmented using the SLS approach (Roura et al., 2015) and estimated lesion masks were afterwards lesion filled using the SLF method (Valverde et al., 2014). On our proposed pipeline using *MSSEG only T1* and *MSSEG T1 + FLAIR* lesion segmentation and filling was part of the same segmentation method. Manual lesion annotations were used to refill T1-w images on pipelines *FAST GT*, *SPM12 GT* and *MSSEG GT* before segmenting the images using *FAST*, *SPM12* and *MSSEG*, respectively.  $AVD_c$  and  $PMC_c$  scores were then computed between pipelines 1 vs 3, 2 vs 3, 4 vs 6, 5 vs 6, 7 vs 9 and 8 vs 9.

Pipeline	Modality	Lesion seg.	Lesion filling	Tissue seg.
1. FAST only T1	T1	none	none	FAST
2. FAST + SLS	T1, FLAIR	SLS (FLAIR)	SLF	FAST
3. FAST GT	T1	expert manual	SLF	FAST
4. SPM12 only T1	T1	none	none	SPM12
5. SPM12 + SLS	T1, FLAIR	SLS (FLAIR)	SLF	SPM12
6. SPM12 GT	T1	expert manual	SLF	SPM12
7. MSSEG only T1	T1	internal	internal	MSSEG
8. MSSEG T1 + FLAIR	T1, FLAIR	internal	internal	MSSEG
9. MSSEG GT	T1	expert manual	SLF	MSSEG

from the brainmask. N3 was run with optimized parameters by reducing the smoothing distance parameter to 30–50 mm (Boyes et al., 2008; Zheng et al., 2009).

The SLF lesion filling method was run with default parameters in all experiments. In the FAST and SPM12 images where we estimated lesion masks automatically, the lesion segmentation method SLS was optimized for 3.0T data identically as shown in Roura et al. (2015).

All the parameters of our proposed method were fixed to default values ( $q = 2$ ,  $\gamma = 0.1$ ,  $w = 1$ ) as done in MR-BrainS13 database. The  $\beta$  parameter was computed automatically. The  $\alpha$  parameter that scaled the minimum signal intensity on the  $H^F$  mask was set again to  $\alpha = 3$ .

### 3.3. Statistical significance

The statistical significance of the performance between methods was computed by running a series of permutation tests (Menke and Martinez, 2004; Klein et al., 2009; Diez et al., 2014) between the differences in the scores obtained by each method. These tests permitted to analyze the fraction of times that a particular method with the lowest score was significantly better than the rest of methods with  $p\text{-value} \leq 0.05$ . Methods were then ranked in three different levels according to the difference between the mean score of the best method  $\mu_o \pm \sigma_o$  and the distance with respect to the mean scores of the rest of methods. Hence, Rank 1 contained methods with mean scores  $(\mu_o - \sigma_o, \mu_o]$ , Rank 2

contained those with mean scores ( $\mu_o - 2\sigma_o, \mu_o - \sigma_o$ ) and Rank 3 those in the interval ( $\mu_o - 3\sigma_o, \mu_o - 2\sigma_o$ ) (Klein et al., 2009; Diez et al., 2014; Valverde et al., 2015a). For all the run tests, we set the number of comparisons between each pair of methods to  $N = 1000$ .

### 3.4. Implementation details

The proposed pipeline was entirely developed in MATLAB (v2014a, The Mathworks Inc, US), except for the registration process that was run using the available NiftyReg package (Ourselin et al., 2002; Modat et al., 2010). The method was configured to run either in CPU or GPU. Experiments were carried out on a GNU/Linux machine with a single Intel core i7 processor at 3.4 Ghz (Intel Corp, US), and a NVIDIA K40 with 12GB of RAM (NVIDIA, US). The average execution time for the proposed method including registration and tissue segmentation was 8 minutes running on the CPU core. Execution time on the GPU was approximately 2 minutes, reducing four times the execution time on the CPU processor.

## 4. Results

### 4.1. MRBrainS13 dataset

Table 2 shows the obtained mean  $DSC_c$ ,  $h_c^{95}$  and  $AVD_c$  scores for our proposed method. We compare the obtained scores with other non-supervised strategies that also participated in the challenge such as FAST, SPM12, or VBM12<sup>7</sup>, and also with respect to the best ranked method proposed by Stollenga and Byeon (2015). The overall rank of methods also included the combined brain (GM + WM) and intracranial (CSF + GM + WM) volumes, which are not shown in the table for simplicity<sup>8</sup>. At the time of submitting our results on the online application, our proposed approach using both T1 and FLAIR (*MSSEG T1+FLAIR*) was the best unsupervised method of the challenge (7th position overall 31 participants), and its accuracy was also very competitive in comparison with several supervised methods that were explicitly trained for the challenge. When only using the T1-w modality

(*MSSEG only T1*), the method was ranked in the 10th position, but still clearly over-performed *FAST* (21th position), and *SPM12* using FLAIR+T1 (17th position), the T1-IR modality (18th position), or the T1-w modality (20th position).

Figure 4 illustrates the different steps performed by our approach. After registering the probabilistic atlases into the subject space (Fig.4 panels E to H), tissue was estimated from the T1-w into 5 different classes (Fig.4 panel I). Then, WM outliers were estimated on the T1-w image by analyzing all the regions not initially segmented as WM with a high probability to pertain to WM based on spatial local probability and prior tissue information (red regions depicted in Fig.4 panel J). If FLAIR was also provided, lesion candidates were also analyzed based on their signal intensity on the FLAIR image and their spatial local probability to pertain to WM (green regions depicted in Fig.4 panel J). Afterwards, lesion candidate regions were refilled into the T1-w image with signal intensities similar to the WM, the refilled T1-w image was re-estimated again and CSFGM and GMWM volumes were reassigned into the three main classes (Fig.4 panels K and L).

### 4.2. MS data

Table 3 (a) depicts the mean % of absolute differences in CSF, GM and WM volume ( $AVD_c$ ) for each of the evaluated methods after segmenting the 24 3T images. Table 3 (b) shows the mean % of mis-classified CSF, GM and WM voxels ( $PMC_c$ ) for each of the evaluated methods.

Methods were ranked based on their scores after running the permutation tests. Table 4 shows the rank of each evaluated method for the  $AVD_c$  (Table 4 (a)) and  $PMC_c$  scores (Table 4 (b)), respectively. The differences in tissue volume were the lowest when methods used also the FLAIR image to estimate the WM outliers. Our proposed approach reported competitive results and again was ranked in the first rank of methods for all tissues. Methods using only T1 yielded a significant higher difference in GM and WM volume and were ranked in the second and third group. The proposed approach using only T1-w was significantly better than the rest of methods in terms of the % of miss-classified GM and WM voxels, but its performance was worst for WM and was ranked in the second group of methods for WM. As shown in Table 4 (a), the % of miss-classified WM voxels was significantly lower in *FAST+SLS* and our proposed method

<sup>7</sup><http://www.neuro.uni-jena.de/>

<sup>8</sup>Overall ranking of methods for all the measurements can be consulted at <http://mrbrains13.isi.uu.nl/results.php>

Table 2: Segmentation results on the 15 test images of the MRBrainS challenge. Mean  $DSC_c$ ,  $h_c^{95}$  and  $AVD_c$  scores for CSF, GM and WM tissue are shown for our proposed method when using only the T1-w modality (*MSSEG only T1*) and when using the T1-w and FLAIR modalities (*MSSEG T1+FLAIR*). The obtained values are compared with the best approach at the time of writing this paper (Stollenga and Byeon, 2015), and also with other unsupervised techniques that also participated in the challenge such as *FAST*, *SPM12* and *VBM12*. The overall ranking of the methods in the challenge is shown in the last column.

Method	$DSC_c$			$h_c^{95}$			$AVD_c$			Rank
	CSF	GM	WM	CSF	GM	WM	CSF	GM	WM	
<b>Best method</b>	$83.72 \pm 2.63$	$84.82 \pm 1.37$	$88.33 \pm 0.89$	$2.14 \pm 0.36$	$1.70 \pm 0.01$	$2.08 \pm 0.33$	$7.09 \pm 4.01$	$6.77 \pm 3.28$	$7.05 \pm 5.22$	1
<b>FAST only T1</b>	$69.95 \pm 2.81$	$78.66 \pm 2.24$	$85.98 \pm 2.58$	$3.41 \pm 0.25$	$4.35 \pm 1.13$	$3.65 \pm 0.85$	$11.83 \pm 10.38$	$8.65 \pm 6.34$	$11.47 \pm 6.24$	21
<b>SPM12 only T1</b>	$70.69 \pm 3.75$	$80.34 \pm 2.37$	$85.58 \pm 1.73$	$5.34 \pm 1.47$	$2.93 \pm 0.25$	$3.06 \pm 0.08$	$23.24 \pm 16.04$	$6.95 \pm 6.57$	$5.99 \pm 3.95$	20
<b>SPM12 T1+FLAIR</b>	$74.03 \pm 3.42$	$81.17 \pm 2.24$	$86.03 \pm 1.48$	$4.59 \pm 0.61$	$2.90 \pm 0.15$	$3.00 \pm 0.07$	$10.07 \pm 4.86$	$10.59 \pm 8.34$	$5.21 \pm 3.88$	17
<b>SPM12 T1-iR</b>	$78.25 \pm 3.78$	$79.41 \pm 2.15$	$83.54 \pm 2.14$	$4.01 \pm 0.63$	$3.01 \pm 0.29$	$3.60 \pm 0.27$	$10.47 \pm 5.69$	$7.23 \pm 6.50$	$6.34 \pm 4.61$	18
<b>VBM12</b>	$74.56 \pm 2.70$	$82.29 \pm 1.49$	$87.95 \pm 1.71$	$3.03 \pm 0.14$	$3.20 \pm 0.32$	$2.32 \pm 0.42$	$6.80 \pm 4.57$	$5.91 \pm 3.91$	$6.06 \pm 4.42$	8
<b>MSSEG only T1</b>	$80.18 \pm 2.67$	$82.06 \pm 1.68$	$87.05 \pm 1.46$	$2.81 \pm 0.21$	$3.33 \pm 0.21$	$2.91 \pm 0.42$	$7.18 \pm 3.33$	$6.15 \pm 3.51$	$6.20 \pm 5.45$	10
<b>MSSEG T1+FLAIR</b>	$80.16 \pm 2.67$	$82.20 \pm 1.60$	$87.33 \pm 1.35$	$2.81 \pm 0.21$	$3.18 \pm 0.15$	$2.88 \pm 0.39$	$7.21 \pm 3.31$	$5.99 \pm 3.43$	$5.95 \pm 5.44$	7

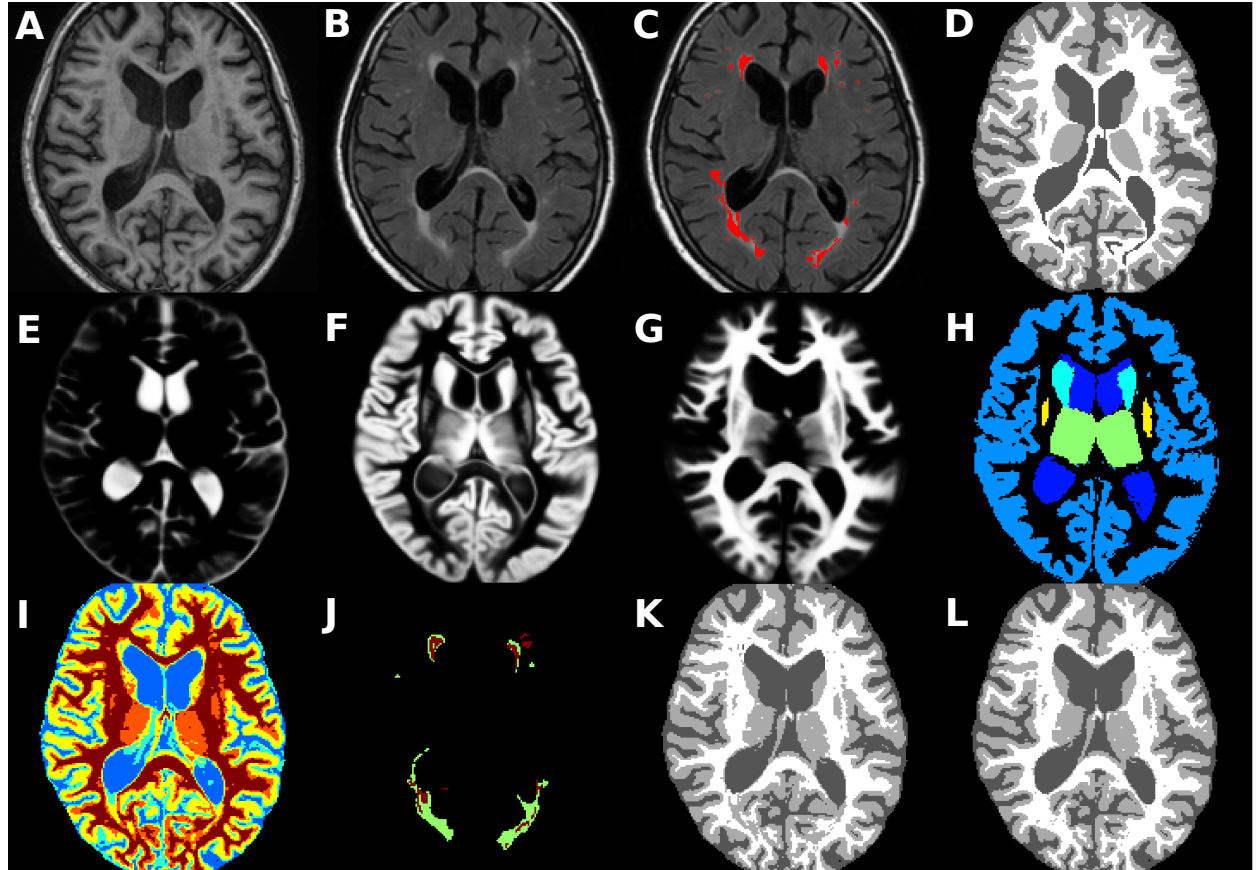


Figure 4: Automated tissue segmentation of the *MSSEG* method on the *second subject* of the training set of the MRBrainS13 database. A) Original T1-w image. B) Original FLAIR image. C) FLAIR image with manual annotated WM lesions depicted in red. D) Provided ground-truth for training purposes. Registered CSF, GM and WM prior atlas to the subject space (E, F and G, respectively). H) Morphological brain structural atlas registered to the subject space. I) First partial volume segmentation with *csf* depicted in blue, *csfgm* in cyan, *gm* in yellow, *gmwm* in orange and *wm* in red. J) Obtained WM outliers extracted from either T1-w (depicted in red) and FLAIR (depicted in green). K) Final tissue segmentation using only the T1-w image, with CSF depicted in dark gray, GM in light gray and WM in white. L) Final tissue segmentation when using both T1 and the FLAIR images.

Table 3: Mean % of absolute difference in CSF, GM and WM volume between the 24 3T tissue masks where expert annotations were refilled before segmentation and the same images segmented including white matter lesions. For each method, reported values are the mean and standard deviation  $\mu \pm \sigma$  for the (a)  $AVD_c$  and (b)  $PMC_c$  scores obtained along the entire database.

(a) Differences in $AVD_c$			
Method	Dif CSF (%)	Dif GM (%)	Dif WM (%)
<b>FAST only T1</b>	$0.07 \pm 0.13$	$0.33 \pm 0.45$	$0.42 \pm 0.56$
<b>FAST + SLS</b>	$0.04 \pm 0.07$	$0.08 \pm 0.12$	$0.11 \pm 0.16$
<b>SPM12 only T1</b>	$0.31 \pm 0.46$	$0.27 \pm 0.45$	$0.56 \pm 0.69$
<b>SPM12 + SLS</b>	$0.22 \pm 0.22$	$0.13 \pm 0.23$	$0.20 \pm 0.32$
<b>MSSEG only T1</b>	$0.13 \pm 0.20$	$0.21 \pm 0.26$	$0.42 \pm 0.54$
<b>MSSEG T1+FLAIR</b>	$0.04 \pm 0.05$	$0.06 \pm 0.05$	$0.13 \pm 0.11$

(b) Differences in $PMC_c$			
Method	CSF (%)	GM (%)	WM (%)
<b>FAST only T1</b>	$0.08 \pm 0.11$	$0.09 \pm 0.12$	$0.53 \pm 0.69$
<b>FAST + SLS</b>	$0.06 \pm 0.06$	$0.14 \pm 0.16$	$0.25 \pm 0.30$
<b>SPM12 only T1</b>	$0.16 \pm 0.32$	$0.25 \pm 0.33$	$0.73 \pm 0.86$
<b>SPM12 + SLS</b>	$0.22 \pm 0.31$	$0.24 \pm 0.29$	$0.41 \pm 0.43$
<b>MSSEG only T1</b>	$0.02 \pm 0.03$	$0.03 \pm 0.05$	$0.46 \pm 0.58$
<b>MSSEG T1+FLAIR</b>	$0.04 \pm 0.04$	$0.14 \pm 0.13$	$0.27 \pm 0.29$

**MSSEG T1+FLAIR** when compared with the rest of evaluated pipelines.

#### 4.2.1. WM outlier rejection

Finally, we evaluated the performance of the proposed WM outlier rejection algorithm with respect to the rest of pipelines. A traditional comparison respect of the number of true-positive and false-positive WM lesion voxels of each pipeline is not appropriate here, given that our approach only processed WM lesion candidates that were not initially classified as WM. In contrast, the error in the expected WM lesion volume segmented can be a good indicator of the performance of each method segmenting WM lesions as WM.<sup>9</sup> Figure 5 shows the % of absolute difference in WM lesion volume between each of the evaluated pipelines and their correspondent  $GT_c^{fill}$  images. As expected, methods yielded the lowest differences in WM lesion volume when used also the FLAIR modality to estimate WM lesions. **MSSEG+FLAIR** showed the lowest differences in WM lesion volume of all evaluated methods.

<sup>9</sup>Aquest punt s'ha de revisar. cal parlar-ne.

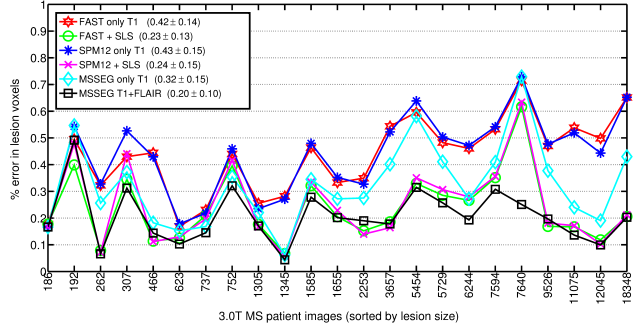


Figure 5: % of absolute difference in WM lesion volume for each of the evaluated pipelines on the 3T MS database. Figure legends also depict mean and standard deviation  $\mu \pm \sigma$  for the entire set of images. Images are sorted by lesion size (number of lesion voxels).

## 5. Discussion

In this paper we have presented a new automated brain tissue segmentation pipeline for MS patient images that combines multi-channel intensities, anatomical and morphological prior maps at different levels to estimate brain tissue in the presence of WM lesions. The current method integrates a WM outlier estimation and refilling algorithm which is applied intermediately in order to reduce the effect of WM lesions on tissue segmentation. As shown by the presented results, the proposed technique yields competitive and consistent results in both general and MS specific databases without parameter tweaking. Furthermore, although we did not analyze explicitly the execution times of each of the evaluated algorithms, the proposed method takes advantage of new affordable processors such as GPUs that reduce up to four times the execution time to register and segment tissue when compared to general purpose CPUs.

The MRBrainS challenge permitted to evaluate the efficacy of our method and to validate it with other state-of-the-art tissue segmentation methods. Although the challenge was not focused on the MS disease, methods were evaluated by comparing them with respect manual expert annotations of tissues and WM lesions, which provided a quantitative measure of the accuracy of the method. The overall results showed that supervised methods obtained the best results of the challenge, taking advantage of the inherent capability to fit the database characteristics. At

Table 4: Permutation tests results for evaluated methods on the 3T MS database. (a) Final rank based on the absolute % difference in CSF, GM and WM volume between methods. (b) Final rank based on % of miss-classified CSF, GM and WM voxels between methods. Reported values are mean and standard deviation ( $\mu_o, \sigma_o$ ) of the fraction of times when each method produces significant p-values ( $p \leq 0.05$ ). Positive values indicate that in average, the method out-performed the other methods in pair-wise significant tests. Negative values indicate the contrary. Rank 1:  $(\mu_o - \sigma_o, \mu_o)$ , Rank 2:  $(\mu_o - 2\sigma_o, \mu_o - \sigma)$ , Rank 3  $(\mu_o - 3\sigma_o, \mu_o - 2\sigma_o)$ . All permutation tests were run with 1000 random iterations.

(a) Evaluated methods ranked by the absolute % of CSF, GM and WM volume of 3T data.						
Rank	Method (CSF)	$\mu \pm \sigma$	Method (GM)	$\mu \pm \sigma$	Method (WM)	$\mu \pm \sigma$
<b>Rank 1</b>	<b>MSSEG T1+FLAIR</b>	$0.5 \pm 0.55$	<b>MSSEG T1+FLAIR</b>	$0.5 \pm 0.55$	FAST + SLS	$0.67 \pm 0.52$
	FAST only T1	$0.5 \pm 0.55$	FAST + SLS	$0.5 \pm 0.55$	<b>MSSEG T1+FLAIR</b>	$0.5 \pm 0.55$
	FAST + SLS	$0.5 \pm 0.55$	SPM12 + SLS	$0.33 \pm 0.52$		
<b>Rank 2</b>	<b>MSSEG only T1</b>	$-0.43 \pm 0.64$	<b>MSSEG only T1</b>	$-0.17 \pm 0.75$	SPM12 + SLS	$0.14 \pm 0.72$
	SPM12 + SLS	$-0.5 \pm 0.55$	SPM12 only T1	$-0.5 \pm 0.55$	FAST only T1	$-0.24 \pm 0.62$
	SPM12 only T1	$-0.57 \pm 0.5$				
<b>Rank 3</b>		FAST only T1		$-0.67 \pm 0.52$	<b>MSSEG only T1</b>	$-0.47 \pm 0.52$
					SPM12 only T1	$-0.59 \pm 0.49$

(b) Evaluated methods ranked by the absolute % of miss-classified CSF, GM and WM of 3T data.						
Rank	Method (CSF)	$\mu \pm \sigma$	Method (GM)	$\mu \pm \sigma$	Method (WM)	$\mu \pm \sigma$
<b>Rank 1</b>	<b>MSSEG only T1</b>	$0.83 \pm 0.41$	<b>MSSEG only T1</b>	$0.83 \pm 0.41$	<b>MSSEG T1+FLAIR</b>	$0.67 \pm 0.52$
	<b>MSSEG T1+FLAIR</b>	$0.44 \pm 0.8$	FAST only T1	$0.5 \pm 0.84$	FAST + SLS	$0.67 \pm 0.52$
<b>Rank 2</b>					SPM12 + SLS	$-0.17 \pm 0.75$
					<b>MSSEG only T1</b>	$-0.17 \pm 0.75$
					FAST only T1	$-0.17 \pm 0.75$
<b>Rank 3</b>	FAST + SLS	$0 \pm 0.89$	FAST + SLS	$-0.17 \pm 0.75$	SPM12 only T1	$-0.83 \pm 0.41$
	SPM12 only T1	$-0.27 \pm 0.43$	<b>MSSEG T1+FLAIR</b>	$-0.17 \pm 0.75$		
	FAST only T1	$-0.33 \pm 0.82$	SPM12 only T1	$-0.33 \pm 0.52$		
	SPM12 + SLS	$-0.67 \pm 0.52$	SPM12 + SLS	$-0.66 \pm 0.51$		

the time of writing this paper, *MSSEG T1+FLAIR* was ranked in the 7th position out of 31 participants, being the best non-supervised strategy followed by the VBM12 approach. As shown by the differences at each of the obtained scores, the FLAIR modality appeared to be useful to improve the accuracy of the method when compared with *MSSEG T1*, which was ranked 10th. The performance of *MSSEG* was superior in all tissues when compared to general purpose methods such as *FAST* (ranked 21th) and *SPM12* (best ranked 17th), even if those used both image modalities. However, final ranking of methods should be taken with care, given the differences in the skull-stripping processes between methods. Differences in the boundaries of the estimated skull masks may be behind the remarkable differences in CSF between methods, altering also the intra-cranial cavity measurements and consequently the overall score of each of the methods.

In MS data, the performance of our method was similar or better to the best pipeline incorporating an state-of-the-art method for lesion segmentation and filling, validating

the overall capability of the proposed method to reduce the effects of WM lesions on tissue segmentation. *MSSEG T1+FLAIR* and *FAST+SLS* were ranked in the first group of methods with error differences in tissue volume below 0.15% in all tissues. Pipelines using only T1-w showed a similar or lower % of miss-classified CSF and GM voxels than those using both FLAIR and T1-w. In contrast, the % of miss-classified WM voxels (Table 4 (a)) and the differences in reassigned lesion volume (Fig. 5) were significantly higher on the former, showing that these methods tended to overestimate GM and underestimate WM by the effect of WM lesions. In this aspect, our results are consistent with previous studies also analyzing the effects of WM lesions on tissue segmentation (Battaglini et al., 2012; Gelineau-Morel et al., 2012; Valverde et al., 2015b,c).

Differences in the  $AVD_c$  between *MSSEG T1+FLAIR* and *MSSEG only T1* on the MRBrains13 data were similar than those reported in MS data, showing that in general the inclusion of the FLAIR modality reduced the overall error in tissue volume on all the analyzed databases. On

MS data, the % of miss-classified CSF and GM voxels was significantly lower on the *MSSEG only T1*, but significantly higher in WM, evidencing that *MSSEG only T1* tended to overestimate WM, while the error in *MSSEG T1+FLAIR* was similar in both GM and WM. In addition, the presented results show that the % difference in total WM and lesion volume was significantly lower on the *MSSEG T1+FLAIR* in comparison with *MSSEG only T1*. Hence, we would recommend to use both T1-w and FLAIR modalities when possible. However, the accuracy of the *MSSEG only T1* pipeline was still superior than *FAST* and *SPM12* when compared with ground-truth annotations of the MRBrainS13 database. This suggests that at least with the available data, the improvement in tissue segmentation was not only caused by the addition of the FLAIR modality, but also by the combination of intensity, anatomical and morphological priors.

This study however endorses some limitations. The lack of a database consisting of MS images with manual annotations of tissue, limits our analysis to the differences in tissue volume with respect to images where expert lesion annotations were lesion filled before tissue segmentation. However, the previous analysis has been shown in previous studies to be effective to evaluate the effects of WM lesions on tissue segmentation (Battaglini et al., 2012; Valverde et al., 2015b,c). Furthermore, the mean lesion sizes of the MS cohorts do not allow to investigate better the performance of the proposed method in the presence of images with higher lesion load. As a future work, we believe that an additional study on MS with manual tissue annotated masks and higher lesion load would be helpful not only to analyze the benefits of the proposed algorithm in MS images, but also to investigate the benefits of adding other image channels such as T2 or PD. Furthermore, although the method was designed for cross-sectional data, we are sensible to the fact that the current approach may be benefited by the possibility to evaluate longitudinal changes in tissue volume.

## 6. Conclusion

In this paper, we have proposed the Multiple Sclerosis SEGmentation pipeline (*MSSEG*), a new MRI brain tissue segmentation method designed to deal with MS patient images containing lesions. Our proposed approach incorporates robust partial volume tissue segmentation

with outlier rejection and filling, combining intensity, probabilistic and morphological prior maps in a novel-way. When combining T1-w and FLAIR modalities, our method have shown very competitive results on the MR-BrainS13 database, ranked on the 7th position out of 31 participant strategies and being the best non-supervised approach so far. In MS data, differences in tissue volume were lower or similar to the best available pipeline composed of *FAST* and a state-of-the-art method for lesion segmentation and filling. In all the experiments the inclusion of the FLAIR modality into the proposed method reduced the effect of WM lesions on tissue segmentation, which suggests that this modality should be used when available. In conclusion, our results show that at least with the presented data, *MSSEG* improves the measurement of brain tissue volume on images containing WM lesions. Hence, we strongly believe that the neuro-image community can be benefited by its use in future settings.

## Acknowledgements:

S. Valverde holds a FI-DGR2013 grant from the Generalitat de Catalunya. E. Roura holds a BR-UdG2013 grant. This work has been partially supported by "La Fundació la Marató de TV3", by Retos de Investigación TIN2014-55710-R, and by the MPC UdG 2016/022 grant. The authors gratefully acknowledge the support of NVIDIA Corporation with the donation of the Tesla K40 GPU used for this research.

## References

- Ashburner, J. and Friston, K. J. (2005). Unified segmentation. *NeuroImage*, 26:839–851.
- Battaglini, M., Jenkinson, M., Stefano, N. D., and De Stefano, N. (2012). Evaluating and reducing the impact of white matter lesions on brain volume measurements. *Human Brain Mapping*, 33(9):2062–71.
- Boyes, R. G., Gunter, J. L., Frost, C., Janke, A. L., Yeatman, T., Hill, D. L. G., Bernstein, M. A., Thompson, P. M., Weiner, M. W., Schuff, N., Alexander, G. E., Killiany, R. J., DeCarli, C., Jack, C. R., and Fox, N. C. (2008). Intensity non-uniformity correction using N3 on 3-T scanners with multichannel phased array coils. *NeuroImage*, 39:1752–1762.

- Cabezas, M., Oliver, A., Lladó, X., Freixenet, J., and Bach Cuadra, M. (2011). A review of atlas-based segmentation for magnetic resonance brain images. *Computer Methods and Programs in Biomedicine*, 104(3):e158–e177.
- Ceccarelli, A., Jackson, J. S., Tauhid, S., Arora, A., Gorky, J., Dell’Oglio, E., Bakshi, A., Chitnis, T., Khouri, S. J., Weiner, H. L., Guttmann, C. R. G., Bakshi, R., and Neema, M. (2012). The impact of lesion inpainting and registration methods on voxel-based morphometry in detecting regional cerebral gray matter atrophy in multiple sclerosis. *American Journal of Neuroradiology*, 33(8):1579–85.
- Chard, D. T., Jackson, J. S., Miller, D. H., and Wheeler-Kingshott, C. A. M. (2010). Reducing the impact of white matter lesions on automated measures of brain gray and white matter volumes. *Journal of Magnetic Resonance Imaging*, 32:223–228.
- Datta, S. and Narayana, P. a. (2013). A comprehensive approach to the segmentation of multichannel three-dimensional MR brain images in multiple sclerosis. *NeuroImage: Clinical*, 2:184–96.
- De Boer, R., Vrooman, H. a., van der Lijn, F., Vernooij, M. W., Ikram, M. A., van der Lugt, A., Breteler, M. M. B., and Niessen, W. J. (2009). White matter lesion extension to automatic brain tissue segmentation on MRI. *NeuroImage*, 45(4):1151–61.
- de Bresser, J., Portegies, M. P., Leemans, A., Biessels, G. J., Kappelle, L. J., Viergever, M. a., Bresser, J. D., and Jan, G. (2011). A comparison of MR based segmentation methods for measuring brain atrophy progression. *NeuroImage*, 54(2):760–8.
- DellOglio, E., Ceccarelli, A., Glanz, B. I., Healy, B. C., Tauhid, S., Arora, A., Saravanan, N., Bruha, M. J., Vartanian, A. V., Dupuy, S. L., Benedict, R. H., Bakshi, R., and Neema, M. (2014). Quantification of Global Cerebral Atrophy in Multiple Sclerosis from 3T MRI Using SPM: The Role of Misclassification Errors. *Journal of Neuroimaging*, 25(2):191–199.
- Deshpande, H., Maurel, P., and Barillot, C. (2015). Classification of Multiple Sclerosis Lesions using Adaptive Dictionary Learning. *Computerized Medical Imaging and Graphics*.
- Dice, L. R. (1945). Measures of the amount of ecologic association between species. *Ecology*, 26(3):297–302.
- Diez, Y., Oliver, A., Cabezas, M., Valverde, S., Martí, R., Vilanova, J. C., Ramió-Torrentà, L., Rovira, À., and Lladó, X. (2014). Intensity based methods for brain MRI longitudinal registration. A study on multiple sclerosis patients. *Neuroinformatics*, 12(3):365–379.
- García-Lorenzo, D., Francis, S., Narayanan, S., Arnold, D. L., and Collins, D. L. (2013). Review of automatic segmentation methods of multiple sclerosis white matter lesions on conventional magnetic resonance imaging. *Medical Image Analysis*, 17(1):1–18.
- Gelineau-Morel, R., Tomassini, V., Jenkinson, M., Johansen-berg, H., Matthews, P. M., and Palace, J. (2012). The Effect of Hypointense White Matter Lesions on Automated Gray Matter Segmentation in Multiple Sclerosis. *Human Brain Mapping*, 2814(June 2011):2802–2814.
- Geremia, E., Clatz, O., Menze, B. H., Konukoglu, E., Criminisi, A., and Ayache, N. (2011). Spatial decision forests for MS lesion segmentation in multi-channel magnetic resonance images. *NeuroImage*, 57(2):378–390.
- Giorgio, A. and De Stefano, N. (2013). Clinical use of brain volumetry. *Journal of Magnetic Resonance Imaging*, 37(1):1–14.
- Guizard, N., Coupé, P., Fonov, V. S., Manjón, J. V., Arnold, D. L., and Collins, D. L. (2015). Rotation-invariant multi-contrast non-local means for MS lesion segmentation. *NeuroImage: Clinical*, 8:376–389.
- Harmouche, R., Subbanna, N. K., Collins, D. L., Arnold, D. L., and Arbel, T. (2015). Based on Modeling Regional Intensity Variability and Local Neighborhood Information. *IEEE Transactions on Biomedical Engineering*, 62(5):1281–1292.

- Huttenlocher, D., Klanderman, G., and Rucklidge, W. (1993). Comparing images using the hausdorff distance. *IEEE Transactions on Pattern Analysis and Machine Intelligence*, 15(9):850–863.
- Immerkær, J. (1996). Fast Noise Variance Estimation. *Computer Vision and Image Understanding*, 64(2):300–302.
- Jain, S., Sima, D. M., Ribbens, A., Cambron, M., Maertens, A., Van Hecke, W., De Mey, J., Barkhof, F., Steenwijk, M. D., Daams, M., Maes, F., Van Huffel, S., Vrenken, H., and Smeets, D. (2015). Automatic segmentation and volumetry of multiple sclerosis brain lesions from MR images. *NeuroImage: Clinical*, 8:367–375.
- Jog, A., Roy, S., Prince, J., and Carass, A. (2013). Mr brain segmentation using decision trees. In *Proceedings of the MICCAI Workshops, Challenge on MR Brain Image Segmentation (MRBrainS 13), The Midas Journal*.
- Klauschen, F., Goldman, A., Barra, V., Meyer-Lindenberg, A., and Lundervold, A. (2009). Evaluation of automated brain MR image segmentation and volumetry methods. *Human brain mapping*, 30(4):1310–27.
- Klein, A., Ardekani, B., Andersson, J., Ashburner, J., Avants, B., Chiang, M., Christensen, G., Collins, D., Gee, J., Hellier, P., and Others (2009). Evaluation of 14 nonlinear deformation algorithms applied to human brain MRI registration. *NeuroImage*, 46(3):786–802.
- Klein, S., Staring, M., Murphy, K., Viergever, M. a., and Pluim, J. P. W. (2010). Elastix: A toolbox for intensity-based medical image registration. *IEEE Transactions on Medical Imaging*, 29(1):196–205.
- Lladó, X., Oliver, A., Cabezas, M., Freixenet, J., Vilanova, J. C., Quiles, A., Valls, L., Ramió-Torrentà, L., and Rovira, A. (2012). Segmentation of multiple sclerosis lesions in brain MRI: A review of automated approaches. *Information Sciences*, 186(1):164–185.
- Magon, S., Gaetano, L., Chakravarty, M. M., Lerch, J. P., Naegelin, Y., Stippich, C., Kappos, L., Radue, E.-W., and Sprenger, T. (2014). White matter lesion filling improves the accuracy of cortical thickness measurements in multiple sclerosis patients: a longitudinal study. *BMC Neuroscience*, 15(1):106.
- Menke, J. and Martinez, T. (2004). Using permutations instead of student's t distribution for p-values in paired-difference algorithm comparisons. In *Neural Networks, 2004. Proceedings. 2004 IEEE International Joint Conference on*, volume 2, pages 1331–1335 vol.2.
- Modat, M., Ridgway, G. R., Taylor, Z. A., Lehmann, M., Barnes, J., Hawkes, D. J., Fox, N. C., and Ourselin, S. (2010). Fast free-form deformation using graphics processing units. *Computer methods and programs in biomedicine*, 98(3):278–84.
- Nakamura, K. and Fisher, E. (2009). Segmentation of brain magnetic resonance images for measurement of gray matter atrophy in multiple sclerosis patients. *NeuroImage*, 44(3):769–76.
- Opbroek, A. V., der Lijn, F. V., and Bruijne, M. D. (2013). Automated brain-tissue segmentation by multi-feature svm classification. In *Proceedings of the MICCAI Workshops, Challenge on MR Brain Image Segmentation (MRBrainS 13), The Midas Journal*.
- Ourselin, S., Stefanescu, R., and Pennec, X. (2002). Robust registration of multi-modal images: Towards real-time clinical applications. In *Medical Image Computing and Computer-Assisted Intervention (MICCAI'02*, pages 140–147. Springer.
- Pérez-Miralles, F., Sastre-Garriga, J., Tintoré, M., Arramíbide, G., Nos, C., Perkal, H., Rfo, J., Edo, M. C., Horga, a., Castilló, J., Auger, C., Huerga, E., Rovira, a., and Montalban, X. (2013). Clinical impact of early brain atrophy in clinically isolated syndromes. *Multiple sclerosis (Hounds Mills, Basingstoke, England)*, 19(14):1878–86.
- Pham, D. L. (2001). Spatial Models for Fuzzy Clustering. *Computer Vision and Image Understanding*, 297:285–297.
- Pohl, K. M., Bouix, S., Nakamura, M., Rohlfing, T., McCarley, R. W., Kikinis, R., Grimson, W. E. L., Shenton,

- M. E., and Wells, W. M. (2007). A hierarchical algorithm for MR brain image parcellation. *IEEE transactions on medical imaging*, 26(9):1201–1212.
- Popescu, V., Battaglini, M., Hoogstrate, W. S., Verfaille, S. C. J., Sluimer, I. C., van Schijndel, R. A., van Dijk, B. W., Cover, K. S., Knol, D. L., Jenkinson, M., Barkhof, F., de Stefano, N., Vrenken, H., Barkhof, F., Montalban, X., Fazekas, F., Filippi, M., Frederiksen, J., Kappos, L., Miller, D., Palace, J., Polman, C., Rocca, M., Rovira, A., and Yousry, T. (2012). Optimizing parameter choice for FSL-Brain Extraction Tool (BET) on 3D T1 images in multiple sclerosis. *NeuroImage*, 61:1484–1494.
- Popescu, V., Ran, N. C. G., Barkhof, F., Chard, D. T., Wheeler-Kingshott, C., and Vrenken, H. (2014). Accurate GM atrophy quantification in MS using lesion-filling with co-registered 2D lesion masks. *NeuroImage: Clinical*, 4:366–73.
- Rajchl, M., Baxter, J. S., McLeod, a. J., Yuan, J., Qiu, W., Peters, T. M., and Khan, A. R. (2015). Hierarchical max-flow segmentation framework for multi-atlas segmentation with Kohonen self-organizing map based Gaussian mixture modeling. *Medical Image Analysis*, 000:1–12.
- Roura, E., Oliver, A., Cabezas, M., Valverde, S., Pareto, D., Vilanova, J. C., Ramió-Torrentà, L., Rovira, À., and Lladó, X. (2015). A toolbox for multiple sclerosis lesion segmentation. *Neuroradiology*, 57(10):1031–1043.
- Roy, S., He, Q., Sweeney, E., Carass, A., Reich, D. S., Prince, J. L., and Pham, D. L. (2015). Subject-Specific Sparse Dictionary Learning for Atlas-Based Brain MRI Segmentation. *IEEE J. Biomed. Heal. informatics*, 19(5):1598–609.
- Schmidt, P., Gaser, C., Arsic, M., Buck, D., Förtschler, A., Berthele, A., Hoshi, M., Ilg, R., Schmid, V. J., Zimmer, C., Hemmer, B., and Mühlau, M. (2012). An automated tool for detection of FLAIR-hyperintense white-matter lesions in Multiple Sclerosis. *NeuroImage*, 59(4):3774–3783.
- Shiee, N., Bazin, P.-L., Ozturk, A., Reich, D. S., Calabresi, P. A., and Pham, D. L. (2010). A topology-preserving approach to the segmentation of brain images with multiple sclerosis lesions. *NeuroImage*, 49(2):1524–1535.
- Sled, J. G., Zijdenbos, a. P., and Evans, a. C. (1998). A nonparametric method for automatic correction of intensity nonuniformity in MRI data. *IEEE Transactions on Medical Imaging*, 17(1):87–97.
- Smith, S. M. (2002). Fast robust automated brain extraction. *Human Brain Mapping*, 17:143–155.
- Smith, S. M., Zhang, Y., Jenkinson, M., Chen, J., Matthews, P., Federico, A., and De Stefano, N. (2002). Accurate, Robust, and Automated Longitudinal and Cross-Sectional Brain Change Analysis . *NeuroImage*, 17(1):479–489.
- Sormani, M. P., Arnold, D. L., and De Stefano, N. (2014). Treatment effect on brain atrophy correlates with treatment effect on disability in multiple sclerosis. *Annals of neurology*, 75(1):43–9.
- Stollenga, M. and Byeon, W. (2015). [M] Parallel Multi-Dimensional LSTM, With Application to Fast Biomedical Volumetric Image Segmentation. In *Neural Information Processing Systems Conference*.
- Sweeney, E. M., Shinohara, R. T., Shiee, N., Mateen, F. J., Chudgar, A. a., Cuzzocreo, J. L., Calabresi, P. a., Pham, D. L., Reich, D. S., and Crainiceanu, C. M. (2013). OA-SIS is Automated Statistical Inference for Segmentation, with applications to multiple sclerosis lesion segmentation in MRI. *NeuroImage: Clinical*, 2:402–13.
- Tomas-Fernandez, X. and Warfield, S. K. (2015). A Model of Population and Subject (MOPS) Intensities with Application to Multiple Sclerosis Lesion Segmentation. *IEEE transactions on medical imaging*, 0062(c):1–15.
- Valverde, S., Oliver, A., Cabezas, M., Roura, E., and Lladó, X. (2015a). Comparison of 10 brain tissue segmentation methods using revisited IBSR annotations. *Journal of Magnetic Resonance Imaging*, 41(1):93–101.

- Valverde, S., Oliver, A., Dez, Y., Cabezas, M., Vilanova, J., Rami-Torrentà, L., Rovira, A., and Lladó, X. (2015b). Evaluating the effects of white matter multiple sclerosis lesions on the volume estimation of 6 brain tissue segmentation methods. *American Journal of Neuroradiology*, 36(6):1109–1115.
- Valverde, S., Oliver, A., and Lladó, X. (2014). A white matter lesion-filling approach to improve brain tissue volume measurements. *NeuroImage: Clinical*, 6:86–92.
- Valverde, S., Oliver, A., Roura, E., Pareto, D., Vilanova, J. C., Ramió-Torrentà, L., Sastre-Garriga, J., Montalban, X., Rovira, A., and Lladó, X. (2015c). Quantifying brain tissue volume in multiple sclerosis with automated lesion segmentation and filling. *NeuroImage: Clinical*, 9:640–647.
- Vincken, K. L., Kuijf, H. J., Breeuwer, M., Bouvy, W. H., Bresser, J. D., Alansary, A., Bruijne, M. D., Carass, A., El-baz, A., Jog, A., Katyal, R., Khan, A. R., Lijn, F. V. D., Mahmood, Q., Mukherjee, R., Oproeck, A. V., Paneri, S., Persson, M., Rajchl, M., Sarikaya, D., Silva, C. A., Vrooman, H. A., Vyas, S., Wang, C., Zhao, L., Biessels, G. J., and Viergever, M. A. (2015). MR-BrainS Challenge: Online Evaluation Framework for Brain Image Segmentation in 3T MRI Scans. *Computational Intelligence and Neuroscience*.
- Zhang, Y., Brady, M., and Smith, S. (2001). Segmentation of brain MR images through a hidden Markov random field model and the expectation-maximization algorithm. *IEEE Transactions on Medical Imaging*, 20:45–57.
- Zheng, W., Chee, M. W. L., and Zagorodnov, V. (2009). Improvement of brain segmentation accuracy by optimizing non-uniformity correction using N3. *NeuroImage*, 48:73–83.